N O T E

Quantitative anatomy mimicking slice phantoms

Karthik Gopalan[1] | **Jonathan I. Tamir[1,2]** | **Ana C. Arias[1]** | **Michael Lustig[1]**

[1]Department of Electrical Engineering and Computer Sciences, University of California, Berkeley, CA, USA

[2]Electrical and Computer Engineering, University of Texas, Austin, TX, USA

Correspondence
Michael Lustig, Department of Electrical Engineering and Computer Sciences, University of California, Berkeley, CA, 94720, USA.
Email: mikilustig@berkeley.edu

Purpose: To present a reproducible methodology for building an anatomy mimicking phantom with targeted T_1 and T_2 contrast for use in quantitative magnetic resonance imaging.

Methods: We propose a reproducible method for creating high-resolution, quantitative slice phantoms. The phantoms are created using gels with different concentrations of $NiCl_2$ and $MnCl_2$ to achieve targeted T_1 and T_2 values. We describe a calibration method for accurately targeting anatomically realistic relaxation pairs. In addition, we developed a method of fabricating slice phantoms by extruding 3D printed walls on acrylic sheets. These procedures are combined to create a physical analog of the Brainweb digital phantom.

Results: With our method, we are able to target specific T_1/T_2 values with less than 10% error. Additionally, our slice phantoms look realistic since their geometries are derived from anatomical data.

Conclusion: Standardized and accurate tools for validating new techniques across sequences, platforms, and different imaging sites are important. Anatomy mimicking, multi-contrast phantoms designed with our procedures could be used for evaluating, testing, and verifying model-based methods.

KEYWORDS
3D printing, digital manufacturing, phantom, quantitative

1 | INTRODUCTION

Magnetic resonance imaging (MRI) is a diagnostic tool that provides invaluable clinical information. It can be made sensitive to a variety of biophysical contrast mechanisms including changes in blood oxygenation, flow, diffusion, and differences in soft tissue. While in some cases it is possible to extract quantitative biophysical parameters, standard clinical practice has been predominantly qualitative in nature through contrast weightings. Quantitative imaging could change the way clinicians diagnose, study, and treat diseases. The main drawback of quantitative MRI is the associated long scan time, as multiple measurements must be made to capture

the signal evolutions. In recent years, a large effort has been placed on reducing the acquisition time and improving the robustness of quantitative imaging methods. These approaches take advantage of spatio-temporal modeling, for example, through compressed sensing,[1,2] MR Fingerprinting,[3] and machine learning.[4]

There is a growing need for realistic phantoms to calibrate and validate these new techniques across different sequences, users, and imaging sites. Most MRI phantoms are made with separate compartments that contain aqueous solutions of paramagnetic ions. Each compartment is designed to mimic certain tissue parameters such as T_1, T_2, spin density, and diffusion coefficients. Although these phantoms are very useful,

they are usually constructed with spheres and cylinders and therefore lack the complicated structure seen in real anatomy. This poses a major drawback, as rapid MRI techniques often make strong modeling assumptions in the reconstruction. Using constraints like Total Variation can produce better results on piece-wise constant phantoms than on real anatomy. That is why the reconstruction community has moved towards prototyping their methods on more anatomically realistic digital phantoms. Phantoms with realistic contrasts and anatomical features could reduce the time required for clinical translation of these ideas, as it would allow researchers to prototype and compare their methods before testing on subjects and volunteers.

MRI phantoms typically use chemicals such as nickel chloride, manganese chloride, copper sulfate, and gadolinium chloride to influence a voxel's T_1 and T_2 values. Though many phantoms use 1 chemical, combinations of paramagnetic ions can be used to achieve a wider range of contrasts.[5] Some phantoms use gels, such as agar, to improve structural stability and to mold into more realistic shapes.[6,7] By adjusting the concentration of agar to water, one can vary T_2 without influencing T_1. It has also been reported that combinations of agar and sucrose can be used to alter a phantom's apparent diffusion coefficient (ADC).[8] Polyvinylpyrrolidone (PVP) may also be used to restrict diffusivity.[9]

Russek et al[10] and Keena et al[11] describe the design, construction, and validation of a highly calibrated system phantom and breast phantom intended for mass manufacturing.

These phantoms are becoming the standards for quantitative imaging and are widely used in the field. Though these contributions address a growing need for standardized phantoms, the designs do not include anatomical features and the use of only 1 chemical produced monotonically increasing T_1/T_2 pairs. Many phantoms[12,13] use separate printed compartments to mimic human anatomy. However, phantoms designed with this method cannot reproduce fine structures due to the limitations of 3-dimensional printing. Altermatt et al[7] described a novel approach for producing highly realistic 3D phantoms using anatomically derived silicone molds. By casting agar in the molds, the authors were able to build a multi-compartment 3D phantom. While their method produced exceptional phantoms, the authors described that some of the anatomical detail was lost due to the fragility of the manufacturing technique.

Another category of phantoms is digital, numerical phantoms. They are frequently used to validate segmentation, reconstruction, and physics based algorithms. The Shepp-Logan phantom is a widely used numerical phantom that uses a set of ellipses to mimic human anatomy.[15] The Brainweb database[14,16] is one of the most popular digital phantoms for MRI. The phantom consists of 10 tissue compartments, and can include mixtures of multiple tissues to emulate multi-compartment relaxation. Guerquin-Kern et al. describe an approach for creating numerical phantoms in k-space with arbitrary shapes based on splines, and include a brain phantom containing multiple compartments.[17] Though digital
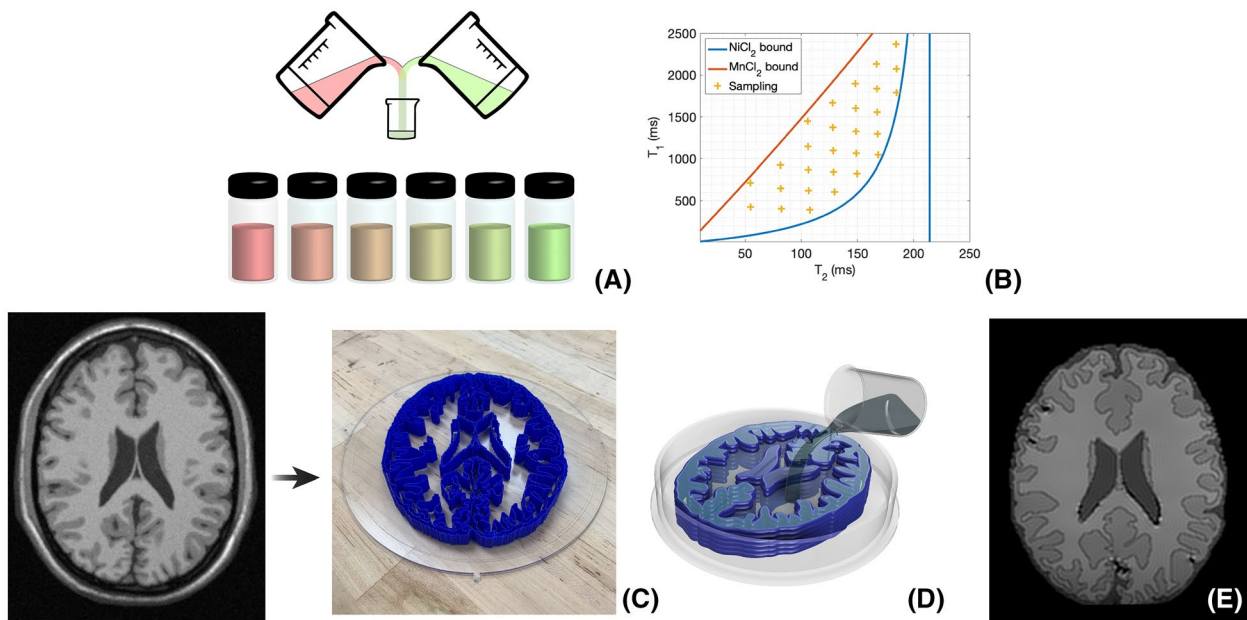
FIGURE 1 Process flow of converting an image of a brain slice into a phantom. A,B, Solutions of paramagnetic ions $NiCl_2$ and $MnCl_2$ are prepared with agar and salt to calibrate the influence of their concentrations on T_1/T_2. C, A slice of a brain is acquired,[14] segmented into compartments, and labeled. The compartment boundaries are 3D printed onto an acrylic sheet. D, Premixed gels are blended following different linear combinations to target specific R1 and R2 values. Different blend compositions are used to fill each compartment according to the anatomy. E, Finally, the phantom is scanned for verification and visualized here with a T_1-weighted image

phantoms are excellent for testing, they cannot model all of the intricacies of scanning a physical object, and they neglect the specific systematic errors present in MR scanners.

In this work, we introduce the idea of converting a digital model into a physical phantom so that any segmented data can be realized as a slice phantom. We describe a process for fabricating realistic slice phantoms with anatomy mimicking T_1 and T_2 contrasts. By deriving a slice phantom from the Brainweb database, we have developed a physical analogue to the digital brain phantom that can be used for actual scanning experiments. The combination of both realistic anatomy and realistic contrast provides a path for creating phantoms that mimic in vivo scanning and bridges the gap between initial prototyping and human subjects testing of new MR acquisitions and reconstructions.

2 | METHODS

The production of a slice phantom requires 3 major steps; gel calibration, digital design, and construction and filling. First, 2 solutions of paramagnetic ions are calibrated to accurately derive the dependence of T_1 and T_2 on their concentrations within a gel (Figure 1A). Our calibration method is a 2- step process in which samples of unknown T_1/T_2 values are prepared, mapped, and fit to a linear model. The parameters from the fit of the crude data are then used to make samples that densely cover the space of attainable T_1/T_2 values. The mapping procedure is repeated in order to improve the linear fit (Figure 1B).

Next, a model of a slice derived from an image, scan data, or vector file is converted into a set of boundaries that will define the walls of the physical phantom (Figure 1C). The boundaries are then 3D printed onto an acrylic sheet to form separate compartments. These compartments are subsequently filled with gels that are prepared from the calibrated solutions (Figure 1D). Finally, the phantom is sealed with a sheet of acrylic and scanned for verification (Figure 1E).

2.1 | Gel preparation and calibration

A combination of agar, $NiCl_2$, $MnCl_2$, NaCl, and deionized water (DIw) is used to target specific T_1/T_2 values. Large stock solutions of $NiCl_2$ and $MnCl_2$ are prepared and stored in airtight containers. The use of solutions is preferred since dry chemicals can absorb moisture and introduce inaccuracies over time. The stock is calibrated by preparing samples with varying concentrations of the solutions mixed with agar gel. The compositions of every sample can be found in Supporting Information Table S1.

All chemicals were acquired from MilliporeSigma (Burlington, MA). Our stock solutions consist of 500 mL of 25 mM $NiCl_2$ and 500 mL of 10 mM $MnCl_2$ in deionized water

(DIw). Larger volumes of water are measured with graduated cylinders (Kimble Kimax, Rockwood, Tennessee). Using an adjustable pipette (Eppendorf, Hamburg, Germany), multiple combinations of each stock solution is added to 20 mL glass vials. Uncertainties were estimated with the manufacturers reported error rates for our equipment. Our pipettes have a systematic error of 0.6% when dispensing 1 mL and an error of 5% when dispensing 20μL. The total volume of each vial is adjusted to 5 mL with DIw. At this stage, the concentrations are arbitrarily chosen. We use a grid of values ranging from 0.4 to 1.2 mL of the $NiCl_2$ solution and from 0.2 to 0.6 mL of the $MnCl_2$ solution. We then prepare a mixture of 300 mL of DIw, 3 g of agar powder (CAS number: 9002-18-0), and 2 g of sodium chloride in a beaker. All solid reagents are weighed with a milligram balance (Mettler Toledo, Columbus, Ohio). The mixture is microwaved for 2-3 minutes until the solution boils and becomes clear. Fifteen grams of the hot gel are added to each vial and thoroughly mixed. The bulk agar gel is covered and placed in a hot water bath in between filling each vial to limit the amount of evaporation.

The samples are then scanned, mapped, and fit to a linear model of R1/R2 vs paramagnetic ion solution volume[5]:

$$\begin{bmatrix} R_1 \\ R_2 \end{bmatrix} = \begin{bmatrix} m_{1,a} & m_{1,b} \\ m_{2,a} & m_{2,b} \end{bmatrix} \begin{bmatrix} k_a \\ k_b \end{bmatrix} + \begin{bmatrix} R_{1,w} \\ R_{2,w} \end{bmatrix}, \quad (1)$$

where R_1 and R_2 are the relaxation parameters in seconds, k_a and k_b are the known solution volumes of the 2 chemicals in mL, and $m_{1,a}, m_{1,b}, m_{2,a}, m_{2,b}, R_{1,w}$, and $R_{2,w}$ are the parameters of the linear fit. Rearranging eqn:linfit, we have

$$\begin{bmatrix} R_1 \\ R_2 \end{bmatrix} = \begin{bmatrix} k_a & k_b & 0 & 0 & 1 & 0 \\ 0 & 0 & k_a & k_b & 0 & 1 \end{bmatrix} \begin{bmatrix} m_{1,a} \\ m_{1,b} \\ m_{2,a} \\ m_{2,b} \\ R_{1,w} \\ R_{2,w} \end{bmatrix} \quad (2)$$

After an initial fit based on a small sample size of arbitrary mixtures, the procedure is repeated by uniformly sampling the space of attainable T_1/T_2 pairs to derive a more accurate fit. To reliably solve for the 6 unknowns, we use 28 unique mixtures. By using our calibration procedure, the T_1 and T_2 values are not dependent on making a solution of a specific molarity which is what most phantom literature reports. Accurately making a solution of a specific molar concentration requires specialized glassware. The calibration method permits the use of volumetric measurements to determine T_1/T_2. Care must be taken to ensure that the temperature remains the same, otherwise it would be possible to perform the calibration using the masses of the solutions. Supporting Information Figure S1 depicts the
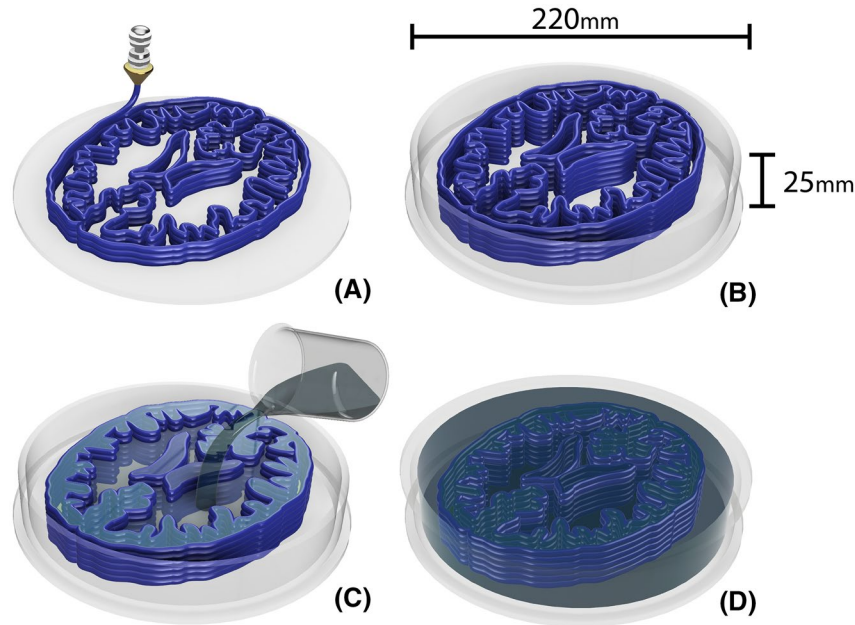
FIGURE 2   A, Each compartment wall is 3D printed directly onto an acrylic base. B, The walls are then sealed with an aerosol sealant like acrylic or polyurethane and a surrounding acrylic ring is attached. C, The compartments of the phantom are then filled with gels with anatomically mimicking T_1/T_2 contrasts. D, The surrounding compartment is filled and the phantom is sealed by attaching an acrylic sheet with acrylic cement

full process of calibration. The red and blue curves represent the extrapolated T_1 and T_2 values achievable when a single chemical solution is used. Using the linear model parameters, targeted values are chosen, mixed, and mapped, demonstrating the ability to target specific relaxation values. Once the model is validated, gels are created to mimic the relaxation times of human anatomy found in the literature.[18]

To derive the relaxation fit, we scanned vials filled with the prepared gel mixtures. The vials were placed in a bath of water to reduce temperature variation and sudden changes in susceptibility. To estimate T_1, a single slice was scanned with a slice-selective inversion recovery spin echo (IR-SE) sequence using a repetition time (TR) of 15 seconds and inversion times (TI) of 100, 500, 900, 1300, and 2000 ms. To estimate T_2, the same slice was scanned with a multiple pure spin echo (SE) sequences with echo times (TE) of 10, 25, 50, 75, 120 ms. Scans were performed with a Siemens 3T Trio (Siemens, Erlangen, Germany) scanner using a commercial 12-channel birdcage head coil. All scans were performed with a 4-mm slice thickness and in-plane resolution of 256 × 256. The field of view (FOV) depended on the arrangement and number of vials, but was typically around 140 mm.

After scanning, the raw, complex-valued data were analyzed in Matlab (Mathworks, Natick, MA). A boundary-labeling algorithm was used to draw regions of interest (ROI) around each vial. The background along with the edges of the vials were then masked to reduce noise. Outlier pixels beyond 99% of the median intensity were removed from each ROI. The remaining pixels within the ROIs were then used to estimate T_1 with an algorithm described in[19] and to estimate T_2 with a nonlinear least squares fit. All mapping was performed on the complex-valued data to reduce bias in the fits due to noise. Following the mapping, Equation (2) was solved to derive the model parameters for the stock solution volume versus R1 and R2.

2.2 | Digital model creation

The digital model for the slice phantom can be derived from any image or vector file and prepared for digital fabrication. Supporting Information Figure S2 shows the process using a slice from the 3D Brainweb data[14]. An axial slice from the Brainweb digital phantom is shown in Supporting Information Figure S2A. The segmented areas of the phantom outside the brain, including the skull and skin, are removed with a masking region. The boundaries of the desired slice are automatically labeled with Matlab's image processing toolkit and are displayed as black borders in Supporting Information Figure S2B. Boundaries with perimeters below a certain threshold are discarded. Some of the boundaries are offset and trimmed to avoid intersections. Finally, the slice boundaries are directly converted to a standard dialect of GCode to be interpreted by a 3D printer. The toolpath is depicted in Supporting Information Figure S2C.

2.3 | Phantom fabrication

Each slice phantom is composed of 3D printed internal structures, gel, and an acrylic enclosure. Polylactic Acid (PLA,

Hatchbox3D) filament is printed directly onto a 3 mm thick acrylic circle (Figure 2A). PLA forms a strong bond with the acrylic and permits the printing of subsequent layers. The 0.45-mm thick walls are printed to a height of 10-15 mm, as shown in Figure 2B. The resolution of the method is limited to the resolution of the 3D printer used. We used a custom built 3D printer, though many commercially available printers would work. The base and walls are then sprayed with a commercially available sealing spray (Rust-Oleum, Extra Cover, Satin Clear) to fill in any gaps inherent to 3D printing. A 25-mm tall acrylic ring is attached to the base with acrylic cement (TAP Plastics, El Cerrito, California). Figure 2C illustrates how each compartment of the phantom is filled with the appropriate gel to target specific T_1/T_2 values derived from the literature.[18] After the gels are prepared, they are allowed to cool until they are below or near the glass transition temperature of PLA, around 65°C. A beaker is used to fill larger compartments while a syringe is used to fill the smaller cavities. Compartments that are too small can be challenging to fill by hand. Once the gels cool, the phantom is sealed by solvent welding a second acrylic circle to the top of the acrylic ring as shown in Figure 2D.

3 | RESULTS

Figure 3 shows the results of the experiment performed after the calibration procedure. The data are obtained by preparing samples to target specific T_1 and T_2 values then scanning and mapping them with the methods described above. These values are also listed in Supporting Information Table S2. The highest error between expected and measured values was 8.6% for T_1 and 9.7% for T_2. We observed that the error in the T_2 measurement generally increased for samples with longer T_2 values and we discuss possible reasons in the following section.

An axial brain slice from the Brainweb database was used to build a slice phantom with the methods described above. The 15-mm tall PLA boundaries took about 2 hours to print onto an acrylic base. The multi-compartment phantom was filled with gels designed to mimic the CSF, gray matter, and white matter. The concentrations used to make vial 13 and vial 8 in Supporting Information Table S2 were used to target gray and white matter, respectively. The CSF was modeled with a lower concentration agar gel (0.5%) with no doping chemicals to have a long T_1 and T_2.
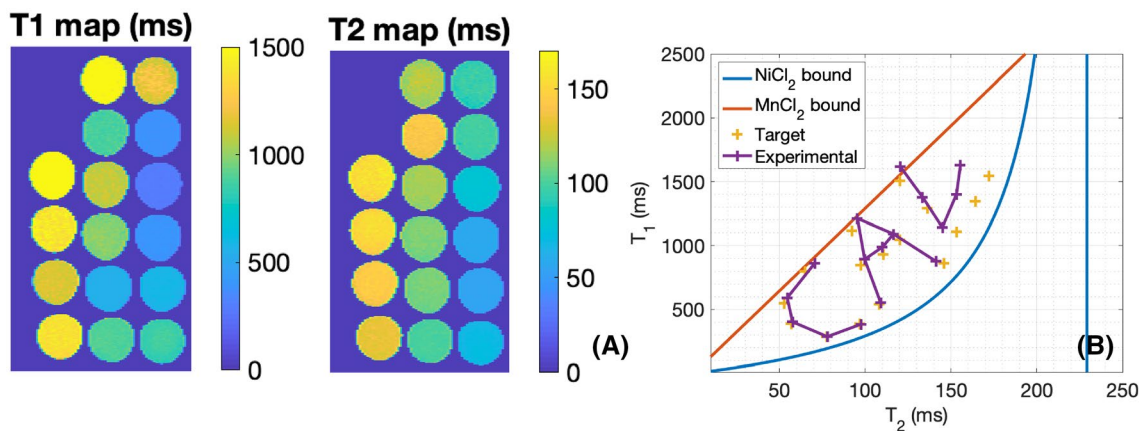
FIGURE 3 A, The parameter maps of samples targeting specific T_1 and T_2 values. B, A plot of the results of the final experiment where targeted values are chosen and samples are mixed and characterized. The experimental values are then compared with the original target values
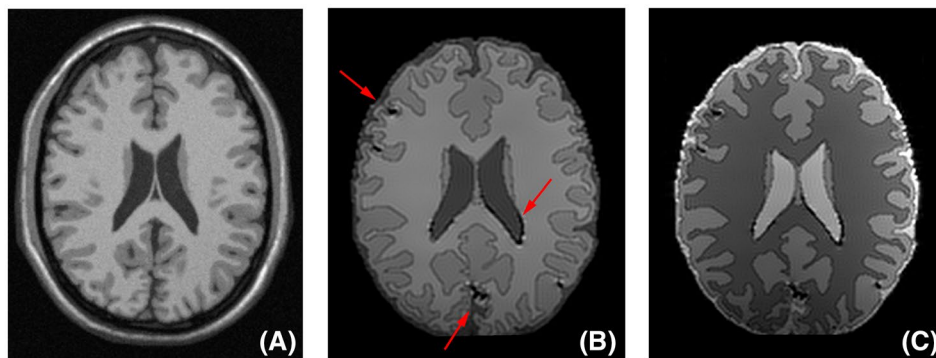
FIGURE 4 A, The T_1 weighted image of the original brainweb model used to design the phantom. B, T_1 weighted IR-SE image of the slice phantom with an inversion time of 2000 ms. Arrows point to susceptibility artifacts due to air bubbles and voids. C, T_2 weighted SE image of the slice phantom with an echo time of 90 ms

Figure 4A depicts a T_1 weighted image of an axial slice of the digital Brainweb model that was used to design the slice phantom. T_1 and T_2 weighted MR scans of the slice phantom are shown in Figure 4B,C, respectively. Though it is missing some of the smaller features, the physical slice phantom appears qualitatively similar to the digital model. The 0.45-mm boundaries between compartments are visible in the scans. Red arrows in Figure 4B depict issues with the construction and filling that resulted in air bubbles within the phantom. Figure 5 showcases another example of a slice
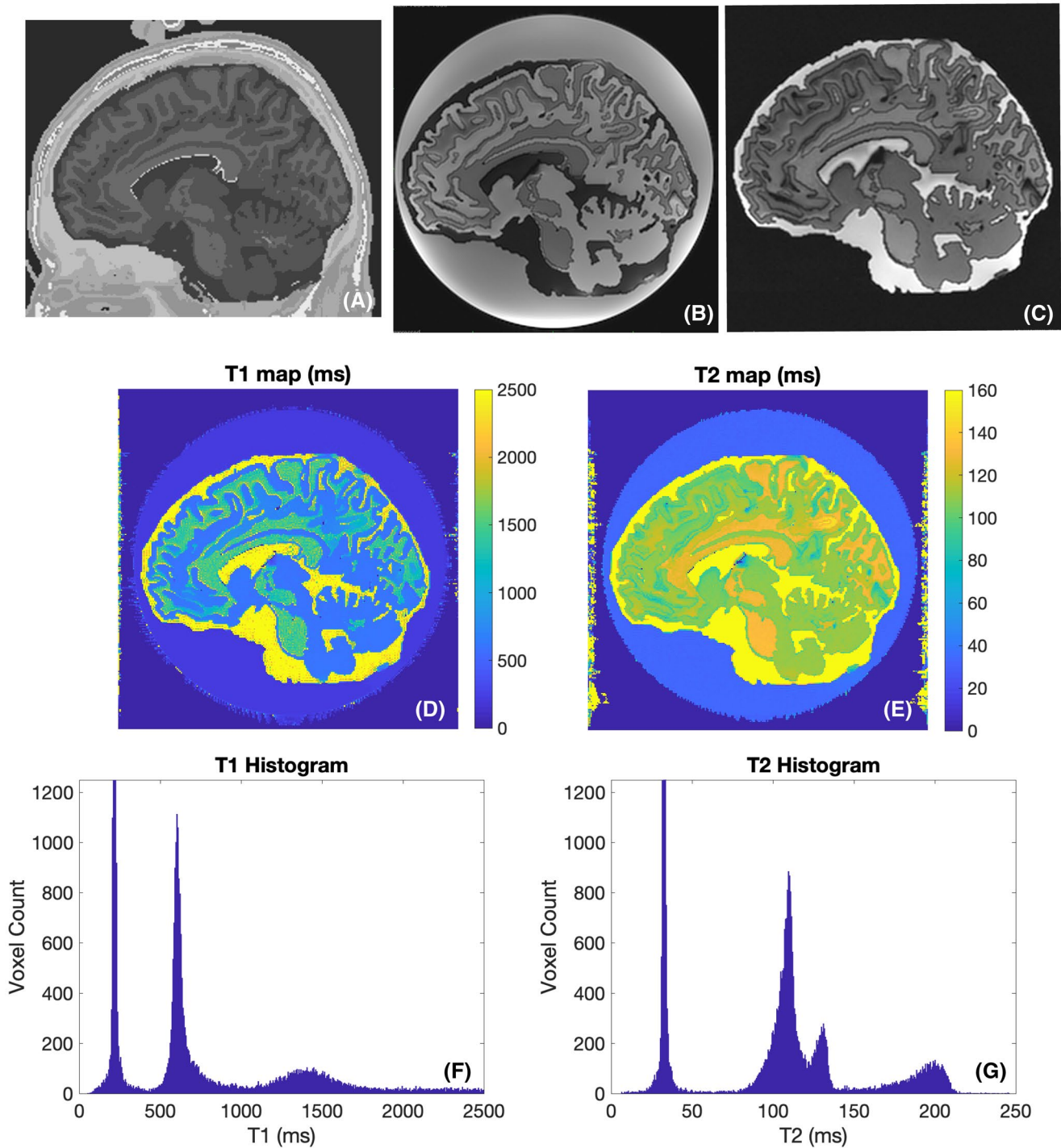
FIGURE 5 A, A sagittal slice of the original brainweb model used to design the phantom. B, T_1 weighted IR-SE image of the slice phantom with an inversion time of 2000 ms and repetition time of 10 000 ms. C, T_2 weighted SE image of the slice phantom with an echo time of 250 ms. D, The T_1 map, E, the T_2 map of the slice phantom as well as relaxivity histograms for (F) T_1 and (G) T_2. Images of this phantom were acquired with a General Electric 750W scanner (GE, Waukesha, Wisconsin). All scans were performed with a repetition time of 10 seconds and a matrix size of 256×256. Seven spin echo sequences were run with echo times of 10, 25, 50, 75, 120, 175, and 250 milliseconds. Inversion recovery spin echo sequences were performed with an echo time of 14 ms and inversion times of 100, 500, 900, 1300, and 2000 milliseconds

phantom made with a sagittal slice from the brain web digital model.

4 | DISCUSSION AND CONCLUSIONS

In this work, we have shown that we can target specific T_1/T_2 values with less than 10% error. We have also presented a method that uses 3D printing to create anatomically realistic phantoms. Our work represents a step toward truly 3D phantoms that would be hard to distinguish from real anatomy by comparing MRI scans. However, the phantoms presented here have limitations. We noticed that T_2 error increases as the target T_2 gets larger. This may be due to the small amounts of solution required to make gels with longer T_2 values (Equation 1) as dispensing small volumes intrinsically has more error. However, the manufacturer reported error rates of our equipment do not account for the measured discrepancies. Different amounts of evaporation during microwaving and handling the gels could cause changes in gel concentration and apparent T_2. In addition, the use of a pure spin echo mapping method could be inaccurate for longer T_2 values since diffusion effects can shorten the apparent T_2. The use of a multi-echo method such as CPMG may reduce the error.[20] Since T_1 and T_2 values are dependent on the measurement methods, effects like magnetization transfer and diffusion can change the relaxation times. While we chose particular sequences and methods for scanning and mapping, there are numerous other techniques that could be used to calibrate the parameters of the phantom. Our phantoms are physical representations of true anatomy and the method that we developed could easily be extended to print structures with arbitrary geometries. This work could be extended by stacking multiple slice phantoms to create a "2.5D" phantom, providing the ability to create high in-plane resolution with varying anatomy across the slice direction.

Our phantoms have not been validated with long-term stability tests. With improper sealing, the agar gel could become dehydrated and change contrast. Acrylic is also not a perfect moisture barrier so some water will leech through over time. PLA is biodegradable and hygroscopic so it may affect the relaxation times of the gels if the sealant fails. In addition, the phantoms have a risk of mold growth if they are not prepared in a sterile environment or mixed with an antibacterial chemical or preservative such as ProClin 150, EDTA, or alcohol. We have also noticed problems with air bubbles. Gases dissolved in the gels can cling to the walls of phantom as the gels cool. These bubbles can lead to susceptibility artifacts as illustrated by red arrows in Figure 4B. This problem could be mitigated by degassing the solutions and preparing the phantoms in a nitrogen environment. Our phantoms only model T_1 and T_2 though

parameters like diffusion, susceptibility, and proton density would be desirable.

We see digital manufacturing playing a large role in the development of MRI hardware. With recent developments in additive processing, high-resolution 3-dimensional phantoms could be printed directly from a scan. Going beyond T_1 and T_2, parameters like diffusion and susceptibility could be modeled and realized with multi material 3D printing. In addition, a phantom that is easy to manufacture could become widely used in the MR community. The work presented here is a small step toward standardized, realistic, and high-quality phantoms.

DATA AVAILABILITY STATEMENT
Scripts and data can be found at https://github.com/mikgroup/phantom-building.

ORCID
Karthik Gopalan http://orcid.org/0000-0001-9836-1944

REFERENCES
1. Lustig M, Donoho D, Pauly JM. Sparse MRI: the application of compressed sensing for rapid MR imaging. *Magn Reson Med*. 2007;58:1182-1195.
2. Doneva M, Börnert P, Eggers H, Stehning C, Sénégas J, Mertins A. Compressed sensing reconstruction for magnetic resonance parameter mapping. *Magn Reson Med*. 2010;64:1114-1120.
3. Ma D, Gulani V, Seiberlich N, et al. Magnetic resonance fingerprinting. *Nature*. 2013;495:187.
4. Wang G, Ye JC, Mueller K, Fessler JA. Image reconstruction is a new frontier of machine learning. *IEEE Trans Med Imaging*. 2018;37:1289-1296.
5. Schneiders NJ. Solutions of two paramagnetic ions for use in nuclear magnetic resonance phantoms. *Med Phys*. 1988;15:12-16.
6. Mitchell MD, Kundel HL, Axel L, Joseph PM. Agarose as a tissue equivalent phantom material for NMR imaging. *Magnetic resonance imaging*. 1986;4:263-266.
7. Altermatt A, Santini F, Deligianni X, et al. Design and construction of an innovative brain phantom prototype for MRI. *Magn Reson Med*. 2018.
8. Lavdas I, Behan KC, Papadaki A, McRobbie DW, Aboagye EO. A phantom for diffusion-weighted MRI (DW-MRI). *J Magn Reson Imaging*. 2013;38:173-179.
9. Pierpaoli C, Sarlls J, Nevo U, Basser PJ, Horkay F. Polyvinylpyrrolidone (PVP) water solutions as isotropic phantoms for diffusion MRI studies Bloch-simulation-based reconstruction. *Proc Int Soc Magn Reson Med*. 2009. Abstract 1414.
10. Russek S, Boss M, Jackson E. Characterization of NIST/ISMRM MRI System Phantom. Proceedings of the 20th Meeting ISMRM, Melbourne. 2012. Abstract 2456.
11. Keenan KE, Wilmes LJ, Aliu SO, et al. Design of a breast phantom for quantitative MRI. *J Magn Reson Imaging*. 2016;44:610-619.
12. Gopalan K, Tamir J, Arias A, Lustig M. Toward 3D printed, anatomy-mimicking, quantitative MRI phantoms. Proceedings of the 25th Meeting ISMRM, Honolulu. 2017. Abstract 3733.
13. Graedel NN, Polimeni JR, Guerin B, Gagoski B, Wald LL. An anatomically realistic temperature phantom for radiofrequency heating measurements. *Magn Reson Med*. 2015;73:442-450.

14. Cocosco CA, Kollokian V, Kwan RKS, Pike GB, Evans AC. Brainweb: online interface to a 3D MRI simulated brain database. *NeuroImage Citeseer*. 1997.

15. Shepp LA, Logan BF. The Fourier reconstruction of a head section. *IEEE Trans Nucl Sci*. 1974;21:21-43.

16. Collins DL, Zijdenbos AP, Kollokian V, et al. Design and construction of a realistic digital brain phantom. *IEEE Trans Med Imaging*. 1998;17:463-468.

17. Guerquin-Kern M, Lejeune L, Pruessmann KP, Unser M. Realistic analytical phantoms for parallel magnetic resonance imaging. *IEEE Trans Med Imaging*. 2011;31:626-636.

18. Wansapura JP, Holland SK, Dunn RS, Ball WS Jr. NMR relaxation times in the human brain at 3.0 tesla. *J Magn Reson Imaging*. 1999;9:531-538.

19. Barral JK, Gudmundson E, Stikov N, Etezadi-Amoli M, Stoica P, Nishimura DG. A robust methodology for in vivo T_1 mapping. *Magn Reson Med*. 2010;64:1057-1067.

20. Ben-Eliezer N, Sodickson DK, Block KT. Rapid and accurate T_2 mapping from multi-spin-echo data using Bloch-simulation-based reconstruction. *Magn Reson Med*. 2015;73:809-817.

SUPPORTING INFORMATION

Additional Supporting Information may be found online in the Supporting Information section.

FIGURE S1 Blue and red lines represent the extrapolated T_1/T_2 values achievable with $NiCl_2$ or $MnCl_2$ alone, respectively. A, After an initial experiment with arbitrary mixtures, only a small portion of the space is sampled to achieve a rough approximate of the extrapolated fit. B, The entire mixing, scanning, and mapping procedure is then repeated with a uniform sampling of the attainable T_1/T_2 pairs to derive a more accurate model

FIGURE S2 A, An image or vector file (eg, from an MR scan or digital phantom) is used to create the digital phantom model. B, The image is segmented into compartments, and undesired segments are removed and the boundary of each compartment is labeled and filtered. C, The final boundaries are scaled and converted to a common dialect of GCode to be interpreted by a 3D printer

TABLE S1 Compositions of each vial made with 25 mM solution of nickel chloride and 10 mM solution of manganese chloride. Each vial was also filled with 15 grams of a hot, aqueous mixture of 1% agar and 0.66% NaCl

TABLE S2 Expected and achieved values of T_1 and T_2 using the entire calibration procedure. Results are listed in order of increasing T_1. The vial number corresponds to the number in the Targeting column of Supporting Information Table S1